# Optimizing an undulating magnetic microswimmer for cargo towing

Emiliya Gutman and Yizhar Or*
*Faculty of Mechanical Engineering, Technion - Israel Institute of Technology, Israel*
(Received 28 December 2015; published 13 June 2016)

One of the promising capabilities of magnetic microswimmers is towing a cargo, which can be used for targeted drug delivery or performing tissue biopsy. A key question is what should be the optimal size ratio between the cargo and the swimmer's flexible tail. This question is addressed here for the simplest theoretical model of a magnetic microswimmer undergoing planar undulations—a spherical load connected by a torsion spring to a rigid slender link. The swimmer's dynamic is formulated and leading-order expressions for its motion are obtained explicitly under small-amplitude approximation. Optimal combinations of magnetic actuation frequency, torsion stiffness, and tail length for maximizing displacement, average speed, or energetic efficiency are obtained. The theoretical results are compared with reported experiments in several types of cargo-towing magnetic microswimmers.

DOI: 10.1103/PhysRevE.93.063105

Recent technological progress has enabled manufacturing and operation of microrobotic and nanorobotic swimmers, which are commonly actuated by a time-varying external magnetic field whose direction is either rotating or oscillating in plane [1–3]. The design of such microswimmers is greatly inspired by swimming microorganisms [4], whose motion is governed by low Reynolds number hydrodynamics, where viscous effects dominate while inertial effects are negligible. Three different types of magnetic microswimmers currently exist, listed as follows. The first type is made of a rigid helix, which is possibly connected to a spherical head or cargo. The swimmer is propelled in a corkscrewlike motion under application of a rotating magnetic field, cf. [3]. The second type [5–7] consists of a rigid magnetic head attached to a flexible thin filament, under a magnetic field with a constant component superposed with a rotating component in a perpendicular plane. Under the combined magnetic field, the flexible wire deforms into a constant helical shape and the microswimmer again moves in steady corkscrew motion. The third type of a magnetic microswimmer is actuated by a magnetic field whose direction undergoes periodic oscillations within a plane, which induce planar undulations of the swimmer's shape that result in net propulsion. A pioneering example of this type of microswimmer has been demonstrated by Dreyfus *et al.* [1], which consisted of a chain of magnetized beads connected by DNA links and composing a flexible magnetic tail, which was attached to a red blood cell. Other recent versions of planar microswimmers of this type are the bio-inspired magnetopserm swimmer of Khalil *et al.* [8], as well as the microswimmers of Jang *et al.* [9], which are composed of discrete chains of two or three rigid links connected by flexible hinges, whose dynamics has been studied analytically in Ref. [10] and numerically in Ref. [11].

These three types of microswimmers differ fundamentally in their direction of net motion: for the first swimmer type, the direction is determined only by the handedness of the rigid helix, so that reversing the sense of the rotating magnetic field results in reversing the swimming direction. On the other hand, the second and third types of swimmers with a flexible tail swim towards the direction of the constant component of the magnetic field and orient themselves with the magnetic part at the front. Therefore, the microswimmers in Refs. [6,8,9] move towards their magnetic head while in Dreyfus's microswimmer [1] the nonmagnetic red blood cell is pulled towards the magnetic tail. Another key difference between the three types of magnetic microswimmers is the dependence on actuation frequency $\omega$ of the magnetic field: for the first type of rigid helical swimmer, the forward speed $V$ increases linearly with $\omega$ until reaching an ultimate upper bound at a critical value of $\omega$ called the step-out frequency. On the other hand, the second and third type of swimmers with a flexible tail have a resonancelike frequency dependence, where $V$ vanishes for $\omega \to 0$ and $\omega \to \infty$ and attains a maximum for some intermediate frequency.

All these magnetic microswimmers mentioned above have a promising potential in modern biomedicine, for performing various minimally invasive tasks inside the human body in the blood vessels, digestive system, or even inside the brain [12]. Importantly, many of these biomedical tasks require capabilities of towing a cargo, which may be a small capsule for targeted drug delivery, a tiny camera for transmitting images, or even tools for taking biopsies of small tissue samples [13]. Basic capabilities of cargo towing have been already demonstrated for all three types of magnetic microswimmers. For the first type of a rigid helical swimmer, Tottori *et al.* [14] have developed a microgripper that can be used for capturing and transporting small particles. For the second type of a corkscrew-rotating swimmer with a flexible tail, Gao *et al.* [6] have demonstrated controlled drug delivery by a spherical capsule attached to the swimmer's magnetic head. For the third type of a planar undulating swimmer, the red blood cell of Dreyfus's microswimmer [1], or the magnetic head of magnetosperm [8] can be regarded as a cargo towed by the flexible tail.

An important aspect of cargo towing by a microswimmer is finding the desired ratio between sizes of the propelling tail of the swimmer and that of the cargo. This question has been addressed by Raz and Leshansky [15] for a theoretical model of internally powered microswimmer with a fixed shape, such as a treadmilling torus or rotating beads, where the optimal size ratio for maximal energetic efficiency has been obtained. Golestanian [16] and Felderhof [17] considered extensions of the three-linked-spheres model [18] where one of the

*izi@tx.technion.ac.il

 

spheres represents a cargo, and studied the effects of structural parameters on swimming speed and energetic efficiency. In a more biologically relevant model, Lauga [19] studied a spermlike microswimmer, which consists of a head connected to an internally actuated flexible tail, and found optimal head-tail size ratio that maximizes either swimming speed or energetic efficiency. While the works mentioned above considered internally actuated swimmers, structural optimization of externally actuated magnetic microswimmers has been studied theoretically in Ref. [20] and verified experimentally in Ref. [21] for the first type of rigid helical microswimmers. For the second type of a rotating flexible tail, Gao *et al.* [6] have found the optimal cargo radius for a given tail, which attains maximal distance per cycle. For the third type of magnetic microswimmer under planar undulations, optimal actuation frequency and optimal length of the flexible magnetic tail for towing the red blood cell have been obtained separately in Ref. [22]. In the work [23], the spheroidal shape of a magnetic head is optimized for a given flexible nonmagnetic tail. It is hard to compare between the optimization results of these works since Ref. [6] involves a variable cargo attached to a head with constant magnetization, Ref. [23] assumes a head with volume-dependent magnetization, while Ref. [22] considers a tail with length-dependent magnetization. Additionally, Refs. [6] and [23] study maximization of distance per cycle (scaled speed $V/\omega$) while Ref. [22] studies maximal speed $V$ by separately optimizing either frequency or tail length. None of these works study combined optimization of all swimmer's parameters–actuation frequency, stiffness, and tail-to-head size ratio. Finally, none of these works studied optimization with respect to energetic efficiency. While energy resources from external magnetic field are commonly believed to pose no practical limitation, an important lesson from the experiments in Ref. [9] is that scenarios of excessive heating of the magnetic coils can be observed for large field intensity and/or frequency. Therefore, energy expenditure and energetic efficiency should also be taken into consideration.

The goal of this paper is to complement the works mentioned above by studying systematic optimization of cargo towing of a planar undulating magnetic microswimmer. Instead of modeling a continuous deformable tail as in Refs. [1,8,22], we study a modification of the simple two-link magnetic microswimmer model presented in Ref. [10], which has been demonstrated experimentally in Ref. [9]. The microswimmer model, shown in Fig. 1, consists of a spherical cargo and a slender link, which are connected by a passive revolute joint with a torsion spring that represents the tail's elasticity. The incorporation of elasticity enables this two-link swimmer to overcome the well-known "scallop theorem" coined by Purcell [24] and to generate net motion in spite of the time-reciprocal periodic input. We consider three typical cases, which differ in the links' magnetization: (i) constant magnetization of a variable-length tail; (ii) length-dependent magnetization of the tail as in Refs. [1,22]; and (iii) constant magnetization of a variable-size cargo as in Ref. [6]. Leading-order expressions for the swimmer's motion under small-amplitude oscillations are formulated, in order to obtain optimal combinations of the swimmer's parameters: actuation frequency, stiffness, and tail length, which maximize the

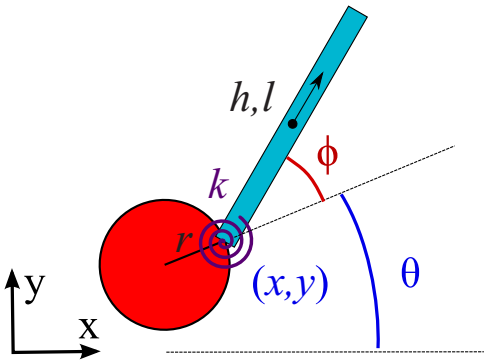


FIG. 1. Two-link model of a magnetic microswimmer with a spherical cargo.

average swimming speed, displacement per cycle, or energetic efficiency. The theoretical results are then compared with reported experimental data on performance of different types of cargo-towing magnetic microswimmers from the literature. Supplemental Material contains MATLAB code for symbolic computation of all the results [25].

The planar microswimmer's model is depicted in Fig. 1. It consists of a spherical cargo of radius $r$ and a slender link of length $l$ and cross-sectional radius $a \ll l$, which are connected by a flexible rotary joint with torsion stiffness constant $k$. The internal torque acting at the flexible joint is given by $\tau = -k\phi$, where $\phi$ is the relative angle at the joint. A planar uniform time-varying external magnetic field is applied, which is given by

$$\mathbf{B}(t) = B_0\{\cos[\psi(t)], \sin[\psi(t)]\}^T, \text{ where } \psi(t) = \varepsilon \sin(\omega t). \tag{1}$$

That is, the magnetic field $\mathbf{B}(t)$ has a constant magnitude of $B_0$ and its direction is oscillating in the $x$-$y$ plane about the $x$ axis at a frequency $\omega$ and angular amplitude of $\varepsilon$. The generalized coordinates that describe the swimmer's planar motion are chosen as $\mathbf{q} = (x, y, \theta, \phi)^T$, where $(x, y)$ denote the position of the joint and $\theta$ is the orientation angle of the spherical cargo, see Fig. 1. For convenience, we first consider case (i) where the slender link has a constant magnetization of strength $h$, which is directed along its longitudinal axis $\hat{\mathbf{t}}$, while the spherical cargo (head) is assumed to be nonmagnetic. The magnetic field generates a time-varying external torque on the slender link, which is given by

$$\mathbf{M}_B(\theta, \phi, t) = h(\hat{\mathbf{t}} \times \mathbf{B}) = hB_0 \sin[\psi(t) - \theta - \phi]\hat{z}. \tag{2}$$

Due to the swimmer's small scale, it is assumed that its motion is governed by low Reynolds number hydrodynamics where viscous drag forces dominate while inertial effects are negligible. The total forces and torques of viscous drag that act on the slender link are approximated by using resistive force theory [26,27], as follows:

$$\mathbf{f}_l = -c_t l(\mathbf{v}_l \cdot \hat{\mathbf{t}})\hat{\mathbf{t}} - c_n l(\mathbf{v}_l \cdot \hat{\mathbf{n}})\hat{\mathbf{n}}$$
$$M_l = -\frac{c_n l^3}{12}\omega_l, \tag{3}$$

where $\mathbf{v}_l$ is the linear velocity of the link's center, $\omega_l$ is its angular velocity about the $z$ axis, $c_t = \frac{2\pi\mu}{\gamma}$ is the viscous resistance in the link's axial direction $\hat{\mathbf{t}}$, and $c_n = 2c_t$ is the viscous resistance in the normal direction $\hat{\mathbf{n}}$. The fluid's viscosity is $\mu$ and the nondimensional constant $\gamma$ depends logarithmically on the link's slenderness ratio as $\gamma = \log(L/a)$ where $L$ is a characteristic length scale [27]. Neglecting hydrodynamic interaction between the cargo and the slender link, the viscous drag forces and torques acting on cargo are given by:

$$\begin{aligned} \mathbf{f}_r &= -6\pi\mu r\mathbf{v}_r \\ M_r &= -8\pi\mu r^3\omega_r, \end{aligned} \tag{4}$$

where $\mathbf{v}_r$ is the linear velocity of the cargo's center, and $\omega_r$ is its angular velocity about the $\hat{z}$ axis.

The dynamic equations of the microswimmer can be obtained by using the assumption of quasistatic motion, which implies that the net forces and torques acting on each link must sum to zero. This gives the following set of equations:

$$\begin{aligned} \mathbf{f}_l + \mathbf{f}_r &= 0 \\ M_r + M_B + M_l + \mathbf{r}_l \times \mathbf{f}_l + \mathbf{r}_r \times \mathbf{f}_r &= 0 \\ M_r + \mathbf{r}_r \times \mathbf{f}_r - \tau &= 0, \end{aligned} \tag{5}$$

where $\mathbf{r}_r$ and $\mathbf{r}_l$ are vectors from the joint to the center of the cargo and center of the tail, respectively. The first equation in (5) is the total force balance on the entire swimmer, which gives two scalar equations in $x, y$ components. The second equation is the $z$ component of torque balance about the joint for the entire swimmer, and the last equation in (5) is the $z$ component of torque balance about the joint for the cargo only, which also counts the internal joint torque $\tau$. Substituting Eqs. (2), (3), and (4) into (5) and expressing $\mathbf{r}_r, \mathbf{r}_l, \mathbf{v}_r$ and $\mathbf{v}_l$ in terms of generalized coordinates and velocities $\mathbf{q}, \dot{\mathbf{q}}$ then yields a 4×4 linear system in $\dot{\mathbf{q}}$, which is given explicitly as:

$$\mathbf{A}(\mathbf{q})\dot{\mathbf{q}} = \mathbf{b}(t, \mathbf{q}), \tag{6}$$

where

$$\mathbf{A}(\mathbf{q}) = \begin{bmatrix} l(1+\sin^2(\theta+\phi))+3\gamma r & -l\sin(\theta+\phi)\cos(\theta+\phi) & -l^2\sin(\theta+\phi)+3\gamma r^2\sin\theta & -l^2\sin(\theta+\phi) \\ -l\sin(\theta+\phi)\cos(\theta+\phi) & l(1+\cos^2(\theta+\phi))+3\gamma r & l^2\cos(\theta+\phi)-3\gamma r^2\cos\theta & l^2\cos(\theta+\phi) \\ -l^2\sin(\theta+\phi)+3\gamma r^2\sin\theta & l^2\cos(\theta+\phi)-3\gamma r^2\cos\theta & 7\gamma r^3+\frac{2}{3}l^3 & \frac{2}{3}l^3 \\ -3\gamma r^2\sin\theta & 3\gamma r^2\cos\theta & -7\gamma r^3 & 0 \end{bmatrix},$$

$$\mathbf{b}(t, \mathbf{q}) = \frac{\gamma}{2\pi\mu}\begin{bmatrix} 0 \\ 0 \\ hB_0\sin(\psi(t)-\theta-\phi) \\ -k\phi \end{bmatrix}.$$

Equation (6) is a coupled nonlinear first-order time-dependent differential equation in $\mathbf{q}(t)$, which governs the microswimmer's motion.

Next, characteristic scales and nondimensional parameters are defined in order to obtain normalized (i.e., dimensionless) equations of motion. Analogously to our previous work [10], we define two characteristic time scales, the viscomagnetic time is $t_m = \frac{8\pi\mu r^3}{3B_0 h}$ and the viscoelastic time $t_k = \frac{\pi\mu r^3}{6k}$. Additionally, we define two nondimensional parameters as $\alpha = t_m/t_k$ and $\delta = l/r$. The equations of motion (6) are then normalized by scaling the time $t$ and frequency $\omega$ with respect to $t_m$ and scaling distances by the radius of the cargo $r$.

We now analyze the swimmer's dynamics assuming small-amplitude oscillations in the direction of the magnetic field, i.e., $\varepsilon \ll 1$ in (1). The solution $\mathbf{q}(t)$ of the (normalized) equations of motion (6) is expanded into a power series in $\varepsilon$ as $\mathbf{q}(t) = \varepsilon\mathbf{q}_1(t) + \varepsilon^2\mathbf{q}_2(t) + \cdots$. Since the expressions in (6) are independent of the position $x, y$ and depend only on the angles $\theta$ and $\phi$, their dynamics is uncoupled and can be analyzed first. The first-order terms in $\varepsilon$ from (6) give the linearized dynamic equations of $\theta_1(t)$ and $\phi_1(t)$ in normalized time as:

$$\begin{bmatrix} \dot{\theta}_1 \\ \dot{\phi}_1 \end{bmatrix} = \begin{bmatrix} A_{11} & A_{12} \\ A_{21} & A_{22} \end{bmatrix}\begin{bmatrix} \theta_1 \\ \phi_1 \end{bmatrix} + \begin{bmatrix} B_1 \\ B_2 \end{bmatrix}\sin(\omega t), \tag{7}$$

where

$$\begin{aligned} A_{11} &= \frac{12\gamma}{\delta(7\delta+24\gamma)} \quad A_{12} = \frac{\alpha\delta^2+6\gamma\alpha\delta+9\gamma\alpha}{12\gamma\delta(7\delta+24\gamma)} \quad A_{21} = \frac{-4\gamma(3\delta^2+14\delta+12\gamma)}{\delta^3(7\delta+24\gamma)} \\ A_{22} &= \frac{-(\alpha\delta^4+6\gamma\alpha\delta^3+18(8\gamma+\gamma\alpha)\delta^2+42(16\gamma+\gamma\alpha)\delta+36\gamma^2\alpha)}{12\gamma\delta^3(7\delta+24\gamma)} \quad B_1 = \frac{-12\gamma}{\delta(7\delta+24\gamma)} \quad B_2 = \frac{4\gamma(3\delta^2+14\delta+12\gamma)}{\delta^3(7\delta+24\gamma)}. \end{aligned} \tag{8}$$

It can be proven that this system is linearly stable for any positive $\alpha$, $\delta$, and $\gamma$, since the eigenvalues of the matrix $[A_{ij}]$ in (7) always have negative real parts. This implies that transient terms in the solution of (7) decay exponentially to zero. Therefore,

we consider only the steady-state solution of (7), which takes the form [25]:

$$\begin{aligned}\theta_1(t) &= C_\theta(\omega,\alpha,\delta)\sin(\omega t) + D_\theta(\omega,\alpha,\delta)\cos(\omega t)\\ \phi_1(t) &= C_\phi(\omega,\alpha,\delta)\sin(\omega t) + D_\phi(\omega,\alpha,\delta)\cos(\omega t).\end{aligned} \tag{9}$$

The first-order dynamics of the swimmer's translation $x, y$ is degenerate $\dot{x}_1 = \dot{y}_1 = 0$. The second-order dynamics of $x(t)$ is given by [25]:

$$\begin{aligned}\dot{x}_2(t) = &-\frac{28\gamma}{\delta(7\delta+24\gamma)}\theta_1^2(t) - \frac{\gamma(\alpha\delta^2+7(16+\alpha)\delta+12(16+\alpha)\gamma)}{4\delta(\delta+3\gamma)(7\delta+24\gamma)}\phi_1^2(t)\\ &- \frac{\gamma(2\alpha\delta^2+(224+7\alpha+6\gamma\alpha)\delta+(528+21\alpha)\gamma)}{4\delta(\delta+3\gamma)(7\delta+24\gamma)}\theta_1(t)\phi_1(t)\\ &+ \frac{28\gamma}{\delta(7\delta+24\gamma)}\sin(\omega t)\theta_1(t) + \frac{4\gamma(7\delta+12\gamma)}{\delta(\delta+3\gamma)(7\delta+24\gamma)}\sin(\omega t)\phi_1(t).\end{aligned} \tag{10}$$

Substituting the solutions of $\phi_1(t)$ and $\theta_1(t)$ from (9) into (10) and integrating in time then gives the steady-state second-order solution of $x(t)$, which takes the form [25]:

$$x_2(t) = C_x(\omega,\alpha,\delta)\sin(2\omega t) + D_x(\omega,\alpha,\delta)\cos(2\omega t) + V_2(\omega,\alpha,\delta)t. \tag{11}$$

Thus, the leading-order expression for the (normalized) mean forward speed of the swimmer is $V = \varepsilon^2 V_2(\omega,\alpha,\delta)$. The net forward displacement per cycle is defined as $X = VT$, where $T = 2\pi/\omega$ is the period time. Explicit leading-order expressions for the speed $V$ and displacement $X$ are obtained as:

$$\begin{aligned}X &= \varepsilon^2\frac{2\pi b_1\omega}{a_4\omega^4 + a_2\omega^2 + a_0} + O(\varepsilon^4)\\ V &= \varepsilon^2\frac{b_1\omega^2}{a_4\omega^4 + a_2\omega^2 + a_0} + O(\varepsilon^4),\end{aligned} \tag{12}$$

where

$$\begin{aligned}b_1 &= 288\alpha\delta\gamma^3(3\delta^2+14\delta+12\gamma)\\ a_4 &= 144\delta^6(7\delta+24\gamma)^2(\delta+3\gamma)\\ a_2 &= [(\delta^4+6\gamma\delta^3+18\gamma\delta^2+42\gamma\delta+36\gamma^2)^2\alpha^2 + 288\gamma^2(3\delta^2+14\delta+12\gamma)^2\alpha + 9216\gamma^2(7\delta+6\gamma)^2](\delta+3\gamma)\\ a_0 &= 16(\delta+3\gamma)(2\delta+3\gamma)^2\alpha^2\gamma^2.\end{aligned} \tag{13}$$

Notice that (12) indicates that the extreme cases of zero or infinite stiffness at the joint ($\alpha \to 0$ or $\alpha \to \infty$) result in zero net motion due to reciprocal motion of $\phi$ and $\theta$ with zero phase difference. (In fact, the work [10] pointed out that a two-link swimmer with $\alpha = 0$ can still swim, provided that the two links both have nonzero and asymmetric magnetization strengths.)

Next, we consider energy expenditure of the microswimmer. The total mechanical work $W$ expended in one period of the swimmer is given by

$$W = \int_0^T P(t)dt = \int_0^{\frac{2\pi}{\omega}} M_B(t)\cdot(\dot{\theta}(t)+\dot{\phi}(t))dt, \tag{14}$$

where $P(t)$ is the instantaneous power expended by the magnetic torque $M_B(t)$. (The same value of $W$ can also be obtained by integrating the power dissipation due to viscous drag forces over one period.) The average power is defined as $\bar{P} = W/T$. Expanding $M_B(t)$ in (2) and substituting the leading-order solution (9) the leading-order expression for $\bar{P}$ can be obtained as [25]:

$$\bar{P} = \varepsilon^2\frac{\frac{16}{3}\pi\gamma((288\delta^3(7\delta+6\gamma)(7\delta+24\gamma)\omega^4 + \alpha^2(2\delta+3\gamma)(\delta^4+6\gamma\delta^3+18\gamma\delta^2+42\gamma\delta+36\gamma^2)\omega^2)}{144\delta^6(7\delta+24\gamma)^2\omega^4 + ((\delta^4+6\gamma\delta^3+18\gamma\delta^2+42\gamma\delta+36\gamma^2)^2\alpha^2 + 288\gamma^2(3\delta^2+14\delta+12\gamma)^2\alpha + 9216\gamma^2(7\delta+6\gamma)^2)\omega^2 + 16\gamma^2(2\delta+3\gamma)^2\alpha^2} + O(\varepsilon^4). \tag{15}$$

Lighthill's energetic efficiency is defined as $\eta = V^2/\bar{P}$, which compares the power required to rigidly dragging the undeformed swimmer by an external force to the actual power required for swimming at the same mean speed. Using (12) and (15), the leading-order expression for Lighthill's efficiency is obtained as

$$\eta = \varepsilon^2\frac{n_2\omega^2}{d_6\omega^6 + d_4\omega^4 + d_2\omega^2 + d_0} + O(\varepsilon^4), \tag{16}$$

where

$$
\begin{aligned}
n_2 &= 15\,552\alpha^2\delta^2\gamma^5(3\delta^2+14\delta+12\gamma)^2\\
d_6 &= 41\,472\delta^9\pi(\delta+3\gamma)^2(7\delta+6\gamma)(7\delta+24\gamma)^3\\
d_4 &= 144\pi\delta^3(7\delta+24\gamma)(\delta+3\gamma)^2[(\delta^4+6\delta^3\gamma+18\delta^2\gamma+42\delta\gamma+36\gamma^2)\\
&\quad\times(28\delta^5+165\delta^4\gamma+(144\gamma+252)\delta^3\gamma+(216\gamma+588)\delta^2\gamma+1008\delta\gamma^2+432\gamma^3)\alpha^2\\
&\quad+576\gamma^2(7\delta+6\gamma)(3\delta^2+14\delta+12\gamma)^2\alpha+18\,432\gamma^2(7\delta+6\gamma)^3]\\
d_2 &= \pi\alpha^2(2\delta+3\gamma)(\delta+3\gamma)^2[(\delta^4+6\delta^3\gamma+18\delta^2\gamma+42\delta\gamma+36\gamma^2)^3\alpha^2\\
&\quad+288\gamma^2(\delta^4+6\delta^3\gamma+18\delta^2\gamma+42\delta\gamma+36\gamma^2)(3\delta^2+14\delta+12\gamma)^2\alpha\\
&\quad+4608\gamma^2(7\delta+6\gamma)(28\delta^5+165\delta^4\gamma+(144\gamma+252)\delta^3\gamma+(216\gamma+588)\delta^2\gamma+1008\delta\gamma^2+432\gamma^3)]\\
d_0 &= 16\alpha^4\gamma^2\pi(\delta+3\gamma)^2(2\delta+3\gamma)^3(\delta^4+6\gamma\delta^3+18\gamma\delta^2+42\gamma\delta+36\gamma^2)
\end{aligned}
\tag{17}
$$

The fact that $\eta$ scales as $\varepsilon^2$ indicates that increasing the actuation amplitude results in larger energetic efficiency. Importantly, the dependence of $X$, $V$, and $\eta$ on the actuation frequency $\omega$ in (12) and (16) indicates that all these quantities vanish at the extreme cases of $\omega \to 0$ and $\omega \to \infty$. Moreover, in the intermediate range there exist different values of optimal frequencies that maximize each of these quantities. As an example, Fig. 2(a) plots $X$, $V$, and $\eta$ as a function of the actuation frequency $\omega$ for $\varepsilon = 0.4$, $\gamma = 3$, $\alpha = 10$, and $\delta = 2$. The dashed curves are leading-order expressions while solid curves are obtained from numerical integration. It can be seen that the leading-order expressions give a very good approximation of the exact quantities for amplitude of $\varepsilon = 0.4$rad. When the amplitude $\varepsilon$ is decreased, deviations between exact values and approximate solutions vanish. It can also be seen that $X$, $V$, and $\eta$ are maximized at different actuation frequencies denoted by $\omega_x$, $\omega_v$ and $\omega_\eta$, respectively. Analytic expressions for these frequencies can be obtained as follows. From (12), the optimal frequency that maximizes the forward speed $V$ is given by

$$
\omega_v = \left(\frac{a_0}{a_4}\right)^{\frac{1}{4}} = \sqrt{\frac{(2\delta+3\gamma)\alpha\gamma}{3(7\delta+24\gamma)\delta^3}}. \tag{18}
$$

The optimal frequency that maximizes the net displacement $X$ is given by

$$
\omega_x = \left(\frac{-a_2+\sqrt{a_2^2+12a_0a_4}}{6a_4}\right)^{\frac{1}{2}}. \tag{19}
$$

Note that $X$ is similar to the scaled speed $V/\omega$, which is considered as a performance measure in several other works, cf. [6]. Using (16), the optimal frequency that maximizes Lighthill's energetic efficiency $\eta$ is obtained as the positive real solution $\omega_\eta$ of the bicubic equation:

$$
2d_6\omega^6 + d_4\omega^4 - d_0 = 0. \tag{20}
$$

It can be verified numerically that the optimal frequency are typically ordered as $\omega_x < \omega_\eta < \omega_v$, as demonstrated in Fig. 2(a).

Next, we consider optimization of other physical parameters of the swimmer, namely the nondimensional stiffness $\alpha$ and tail-cargo size ratio $\delta$, for maximizing either $V$, $X$, or $\eta$. Since the dependence on the slenderness parameter $\gamma$ is less significant, we choose a typical value of $\gamma = 3$, which is adopted from the microswimmers in Ref. [9] and corresponds to slenderness ratio of $L \approx 20a$. Substituting the optimal frequency $\omega = \omega_v$ in (18) into the expression for $V$ in (12) gives:

$$
V(\omega=\omega_v,\alpha,\delta) = \frac{288\gamma^3\delta(3\delta^2+14\delta+12\gamma)\alpha}{(\delta+3\gamma)[(\delta^4+6\gamma\delta^3+18\gamma\delta^2+42\gamma\delta+36\gamma^2)\alpha+672\gamma\delta+576\gamma^2]^2}. \tag{21}
$$

Figure 2(a) shows a contour plot of $V(\omega_v)$ as a function of $\alpha$ and $\delta$ for $\gamma = 3$. It can be seen that for a given value of $\alpha$ there exists an optimal value of $\delta$, and vice versa. Moreover, there exist optimal combination of both parameters for which the speed $V(\omega_v)$ attains a global maximum. This can also be shown analytically, as follows. From (12) and (18), the optimal value of $\alpha$ that maximizes $V(\omega_v)$ for given $\delta$ is obtained as

$$
\alpha_v = \frac{96\gamma(7\gamma\delta+6\gamma^2)}{\delta^4+6\gamma\delta^3+18\gamma\delta^2+42\gamma\delta+36\gamma^2}. \tag{22}
$$

Substituting $\alpha = \alpha_v$ into (21) then gives $V$ as a function of $\delta$:

$$
V(\omega=\omega_v,\alpha=\alpha_v,\delta) = \varepsilon^2\frac{0.75\gamma^2\delta(3\delta^2+14\delta+12\gamma)}{(\delta+3\gamma)(7\delta+6\gamma)(\delta^4+6\gamma\delta^3+18\gamma\delta^2+42\gamma\delta+36\gamma^2)}.
$$

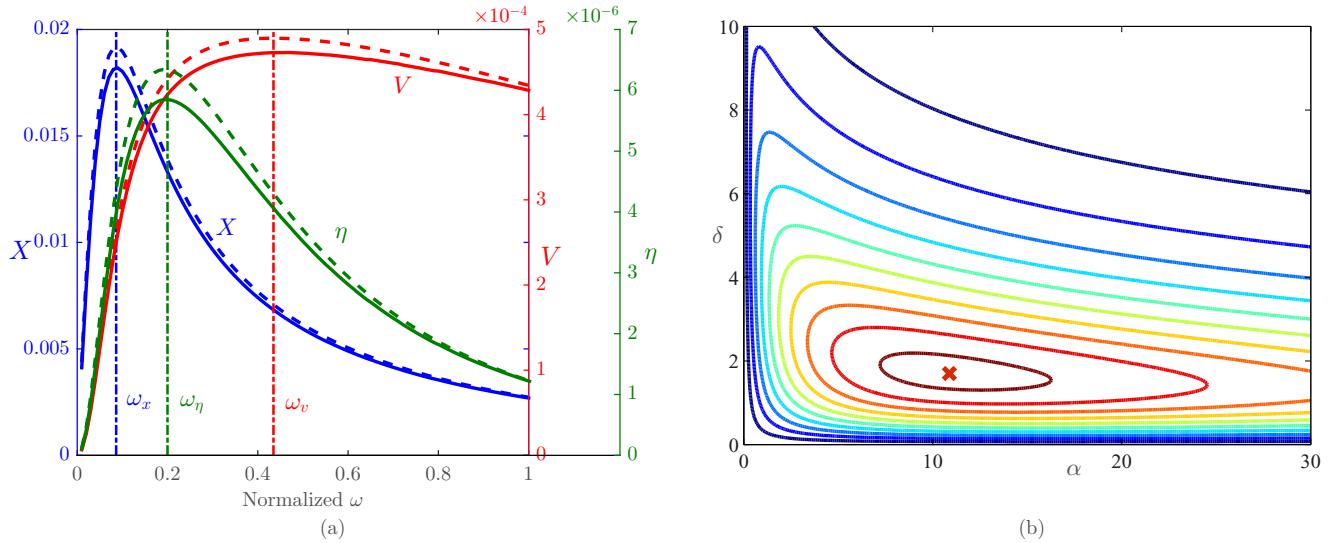


FIG. 2. (a) $X$, $V$ and $\eta$ as a function of $\omega$ for $\varepsilon = 0.4$, $\gamma = 3$, $\alpha = 10$, and $\delta = 2$. The dashed curves are leading-order expressions while solid curves are obtained form numerical integration. (b) Contour lines of mean speed $V(\omega_v)$ for $\gamma = 3$ as a function of $\alpha$ and $\delta$.

For a given value of $\gamma$, the optimal value of the size ratio $\delta$ is obtained by finding the positive real root of an eighth-order polynomial in $\delta$. Choosing $\gamma = 3$, a global maximum for the speed $V_{\max}$ is attained for $\omega_v \approx 0.5713$, $\alpha_v \approx 10.88$, and $\delta_v \approx 1.7016$, such that $V_{\max} = 3.1\times10^{-3}\varepsilon^2\frac{r}{t_m}$. Remarkably, it can be seen that the optimal tail length is shorter than the diameter of the cargo. This is in qualitative agreement with the observation made in Ref. [21] that the optimal helical tail for towing a cargo is very short—just a bit longer than a single pitch of the helix.

Substituting the optimal frequency $\omega = \omega_x$ into the expression for the forward displacement $X$ in (12), it can be shown that for given values of $\delta$ and $\gamma$, maximization of $X(\omega_x)$ is attained at the nonphysical limit of $\alpha,\omega_x \to 0$. The same phenomenon also occurred for the two-link microswimmer model analyzed in Ref. [9]. For given values of $\alpha$ and $\gamma$, the dependence of $X(\omega_x)$ on $\delta$ is complicated. Nevertheless, there is also an optimal value of $\delta$, which maximizes $X(\omega_x)$. For example, choosing $\alpha = \alpha_v = 10.88$ and $\gamma = 3$, one obtains an optimal frequency of $\omega_x = 0.068\,26$ and optimal size ratio of $\delta_x = 3.018$, which gives $X = 125.5\times10^{-3}\varepsilon^2 r$. That is, the optimal tail for maximizing $X$ is longer than the one required for maximizing $V$. For these parameter values the mean speed is indeed suboptimal, $V = 1.36\times10^{-3}\varepsilon^2\frac{r}{t_m} < V_{\max}$.

The expression for Lighthill's efficiency (16) is also maximized at a unique optimal combination of the parameters $\alpha,\delta$, and frequency $\omega$. Finding the optimal value requires solving a complicated set of high-degree polynomial equations. For example, choosing $\gamma = 3$, the optimal (normalized) parameter values are obtained numerically as $\omega_\eta = 5\times10^{-5}$, $\alpha_\eta = 0.0019$, and $\delta_\eta = 2.15$. The optimization results are summarized in Table I (left column). It can be seen that the optimal values of $\alpha$ and $\omega$ for maximizing speed, displacement, or

TABLE I. Summary table.

| Case | (i) Link constant magnetization | (ii) Link length-dependent magnetization | (iii) Head constant magnetization |
|---|---|---|---|
| scaling | $h = \text{const}$<br>$r = \text{const}$<br>$t_k = \frac{\pi\mu r^3}{6k}$<br>$t_m = \frac{8\mu\pi r^3}{3B_0 h}$ | $h = m\cdot l$<br>$r = \text{const}$<br>$t_k = \frac{\pi\mu r^3}{6k}$<br>$t_m = \frac{8\mu\pi r^2}{3B_0 m}$ | $h = \text{const}$<br>$l = \text{const}$<br>$t_k = \frac{\pi\mu l^3}{6k}$<br>$t_m = \frac{8\mu\pi l^3}{3B_0 h}$ |
| $\frac{V_{\text{opt}}}{\varepsilon^2 r/t_m}$ | $\delta_v = 1.7$<br>$\alpha_v = 10.88$<br>$\omega_v = 0.57$<br>$V = 3.1\times10^{-3}$ | $\delta_v = 4.015$<br>$\alpha_v = 17.06$<br>$\omega_v = 0.4243$<br>$V = 8.156\times10^{-3}$ | $\delta_v = 4.92$<br>$\alpha_v = 8.774$<br>$\omega_v = 13.61$<br>$V = -28.7\times10^{-3}$ |
| $\frac{X_{\text{opt}}}{\varepsilon^2 r}$<br>$\alpha = \alpha_v$ | $\delta_x = 3.018$<br>$\omega_x = 0.068\,26$<br>$X = 125.5\times10^{-3}$ | $\delta_x = 7.223$<br>$\omega_x = 0.1039$<br>$X = 253.3\times10^{-3}$ | $\delta_x = 2.622$<br>$\omega_x = 1.61$<br>$X = -45.84\times10^{-3}$ |
| $\frac{\eta_{\text{opt}}}{\mu\varepsilon^2 r^3/t_m^2}$ | $\delta_\eta = 2.15$<br>$\alpha_\eta = 0.0019$<br>$\omega_\eta = 5\times10^{-5}$<br>$\eta = 1.1454\times10^{-4}$ | $\delta_\eta = 2.15$<br>$\alpha_\eta = 0.0019$<br>$\omega_\eta = 5\times10^{-5}$<br>$\eta = 1.1454\times10^{-4}$ | $\delta_\eta = 3.25$<br>$\alpha_\eta = 3\times10^{-5}$<br>$\omega_\eta = 2.2\times10^{-5}$<br>$\eta = 3.3774\times10^{-4}$ |

TABLE II. Swimmer comparison.

| | $B_0$ [mT] | $\varepsilon$ | $r$ [$\mu$m] | $\delta$ | $a$ [$\mu$m] | $h$ or $m$ [Am$^2$] or [$Am$] | $\mu$ [Pa s] | $f$ [Hz] | $V$ [$\mu$m/sec] | $X = V/f$ [$\mu$m] | $V_\alpha$ [$\mu$m/sec] | $X_\alpha$ [$\mu$m] | $\delta_{\text{opt}}$ | $V_{\alpha\delta}$ [$\mu$m/sec] | $X_{\alpha\delta}$ [$\mu$m] |
|---|---|---|---|---|---|---|---|---|---|---|---|---|---|---|---|
| 1. Walker | 4 | – | 0.24 | $\delta_v = 5.5$ | 0.11 | $h = 1.4 \cdot 10^{-16}$ | $10^{-3}$ | $f_v = 80$ | 10.6 | 0.133 | 1.4 | 0.017 | 2.73 | 2.77 | 0.035 |
| 2. Tottori | 1 | – | 3 | 19 | 1 | $h = 2.2 \cdot 10^{-11}$ | $10^{-3}$ | 10 | $25^+$ | 2.5 | 24.5 | 2.45 | 18.18 | 24.53 | 2.45 |
| 3. Dreyfus | 8.9 | 1.16 | 3.1 | 7.7 | 0.5 | $m = 4 \cdot 10^{-6}$ | $10^{-3}$ | $f_x = 10$ | 22 | 2.2 | 24.84 | 2.48 | 29.8 | 42.13 | 4.21 |
| 4. Gao | 1 | 0.811 | 0.625 | $\delta_v = 9.28$ | 0.2 | $h = 9 \cdot 10^{-14}$ | $10^{-3}$ | 10 | 11 | 1.1 | 1.055 | 0.1055 | 2.24 | 3.45 | 0.345 |
| 5. Khalil | 5 | $\pi/4$ | 21.3 | 15.1 | 2.6 | $h = 1.6 \cdot 10^{-7}$ | $10^{-3}$ | $f_v = 45$ | 158 | 3.5 | 139.89 | 3.1 | 0.93 | 2324.57 | 51.6572 |

efficiency differ significantly in several orders of magnitudes. On the other hand, optimal values of the size ratio $\delta$ always remain within $O(1)$.

Next, we consider case (ii) where the tail's magnetization depends linearly on the link's length. This is highly relevant in case where the tail is made of a magnetic material or composed of a chain of magnetic beads as in Refs. [1,22]. Let $m$ denote the link's magnetization per unit length, such that $h = ml$. In this case, we choose a different time scale for normalization as $t'_m = \frac{8\mu r^2}{3B_0 m}$, which is independent of $l$. The new and old time scales are related as $t'_m = \delta t_m$. This affects the definition of normalized frequency and stiffness, which now satisfy $\omega' = \delta\omega$ and $\alpha' = \delta\alpha$. The expressions for the net displacement per period $X$ and Lighthill's efficiency $\eta$ can be directly obtained by substituting $\omega = \omega'/\delta$ and $\alpha = \alpha'/\delta$ into (12) and (16), respectively. The mean speed $V'$ is now normalized by the new time scale $t'_m$, and thus one has to use the relation $V' = \delta V$ in (12) and (23), in addition to the above substitutions. Importantly, despite the fact that the magnetic moment $M_B$ grows linearly in the length $l$, there still exists an optimal size ratio $\delta$, which maximizes either $V'$, $X$, or $\eta$. Optimal values can be obtained similarly to the previous case of constant tail's magnetization, but naturally result in different numerical values due to the different dependence on $\delta$. The optimization results for this case are summarized in Table I (middle column). Notably, the optimal size ratio $\delta$ for maximizing $V$ or $X$ is now significantly larger due to the dependence of the magnetic moment on $\delta$, which changes the tradeoff with increased drag.

We now consider case (iii) of a nonmagnetic tail with a constant length, and a variable-size cargo attached to a small particle with constant magnetization $h$, as in Ref. [6]. This case dictates slight changes in the equations of motion, as follows. First, since the magnetic moment $M_B$ in (2) now acts on the head, it is given as $M_B(\theta,t) = hB_0 \sin[\psi(t) - \theta]$. additionally, the third equation in (5) is changed to $M_r + \mathbf{r}_r \times \mathbf{f}_r - \tau + M_B = 0$. Finally, the right-hand side of (6) is changed to $\mathbf{b}(t,\mathbf{q}) = \frac{\gamma}{2\pi\mu}[0\ 0\ M_B\ \ \tau - M_B]^T$. Since the head size is variable, it is more reasonable to scale distances by the tail's length $l$, and redefine the two characteristic times as $t_m = \frac{8\pi\mu l^3}{3B_0 h}$ and $t_k = \frac{\pi\mu l^3}{6k}$, while the definitions of $\alpha = t_m/t_k$ and $\delta = l/r$ are unchanged. Derivation of the leading-order solution of (6) follows the same process as described above, see Supplemental Material for computational code [25]. The optimization process for maximizing $X$, $V$, or $\eta$ is the same as above (see Ref. [25]), and optimal parameter values are summarized in Table I (right column). Note that in this case the motion is towards the magnetic head, hence $X$ and $V$ are negative.

We now compare the theoretical results of our model to reported experimental results of several cargo-towing magnetic microswimmers, as summarized in Table II. The corkscrewlike microswimmers of Walker *et al.* [21] and Tottori *et al.* [14] are compared to case (i) with constant magnetization and variable tail length. The planar undulating microswimmer of Dreyfus [1] is compared to case (ii) with length-dependent tail magnetization. The flexible helical swimmer of Gao [6] and the planar undulating magnetosperm of Khalil *et al.* [8] are compared to case (iii) of constant head magnetization. The first ten columns in Table II give physical values of the swimmers' parameters and performance. While most of the values are extracted from the cited papers, some of them were estimated due to missing information. Specifically, magnetization values of microbeads in the flexible tail of Ref. [1] were estimated using values for Myone Dynabeads from Ref. [28], and represented as magnetization per unit length $m$. The viscosity of water has been assumed for the microswimmers of Gao [6] and Khalil [8]. Values of the actuation frequency $f$ are given in Hz. Values that have been optimized for $X$ and $V$ are denoted in the table as $f_x$, $\delta_v$, etc. Finally, the amplitude parameter $\varepsilon$ is irrelevant for the helical swimmer, and hence omitted.

The last five columns in Table II show predicted optimal performance of our theoretical model for the same values of the microswimmers' physical parameters. The columns of $V_\alpha$ and $X_\alpha$ denote the maximal speed and displacement in our theoretical model, which are obtained by choosing the optimal value of the stiffness parameter $\alpha$ while using the same frequency $f$ and tail-head size ratio $\delta$ as given in the first ten columns. The next column denotes the optimal size ratio $\delta_{\text{opt}}$ for maximizing both $X$ and $V$, for the same physical values and actuation frequency [according to (12), for a fixed frequency $\omega$ both $X$ and $V$ are maximized for the same combination of $\alpha$ and $\delta$]. Finally, the columns of $V_{\alpha\delta}$ and $X_{\alpha\delta}$ denote the maximal speed and displacement in our theoretical model, which are obtained by optimizing both $\delta$ and $\alpha$.

It can be seen that the results of our theoretical model roughly fall within the same order of magnitude as the experimental microswimmers with planar undulations (third and fifth lines of Table II). There is a much larger discrepancy for some microswimmers with spatial corkscrewlike motion (lines 1 and 5), and it seems that the microswimmer of Gao [6] with helical rotating flexible tail outperforms the planar undulations considered by our model. It is a bit harder to compare the performance of rigid helices (Walker and Tottori) to our model due to the different dependence on frequency, and to the irrelevance of the small amplitude parameter $\varepsilon$ in their

actuation (we arbitrarily chose $\varepsilon = 1$rad for the comparison). As for Dreyfus's undulating microswimmer, our model shows good agreement in $V_\alpha$ and $X_\alpha$. Moreover, it predicts that $X$ and $V$ can be slightly improved by increasing the tail's length $\delta$ for the same values of frequency and magnetization per unit length (as estimated from Ref. [28]). On the other hand, performance of Khalil's magnetosperm [8] seems to be suboptimal since its tail's length appears to be significantly too large. Nevertheless, one cannot expect a perfect quantitative matching between a flexible tail and a rigid link whose flexibility is lumped entirely into a single joint, as in our theoretical model. Finally, it should be noted that our model does not account for hydrodynamic interaction between the cargo and the tail, hence the quantitative accuracy of the result is limited, particularly in cases of a short tail, i.e., $\delta \approx 1$.

In conclusion, we have presented a simple theoretical two-link model of a magnetic microswimmer with a spherical cargo and a slender tail. We have analyzed the swimmer's dynamics and obtained explicit leading-order expressions for its mean speed $V$, displacement $X$, and Lighthill's energetic efficiency $\eta$, under small-amplitude expansion. We found optimal combinations of frequency, stiffness and tail-cargo size ratio for maximizing either $X$, $V$, or $\eta$. Each of these performance measures is maximized at a different range of optimal parameters. We have also demonstrated the importance of the choice of scaling, which must be adapted to the particular type of the microswimmer, depending on its constant and variable physical parameters. We have conducted qualitative order-of-magnitude comparison of our model with several experimental cargo-towing microswimmers. Our work demonstrates the importance of simple low-dimensional models of microswimmers for understanding the qualitative dependence of swimming performance on physical properties of the swimmer and its actuation. Nevertheless, these theoretical models must be augmented with numerical analysis of more detailed and accurate models, as well as quantitative analysis of experimental measurements.

This work is supported by the Israeli Science Foundation (ISF) under Grant No. 567/14.

[1] R. Dreyfus, J. Baudry, M. L. Roper, M. Fermigier, H. A. Stone, and J. Bibette, Microscopic artificial swimmers, Nature (London) **437**, 862, (2005).

[2] K. E. Peyer, L. Zhang, and B. J. Nelson, Bio-inspired magnetic swimming microrobots for biomedical applications, Nanoscale **5**, 1259 (2013).

[3] A. Ghosh and P. Fischer, Controlled propulsion of artificial magnetic nanostructured propellers, Nano Lett. **9**, 2243 (2009).

[4] E. Lauga and T. R. Powers, The hydrodynamics of swimming microorganisms, Rep. Prog. Phys. **72**, 096601 (2009).

[5] U. K. Cheang, D. Roy, J. H. Lee, and M. J. Kim, Fabrication and magnetic control of bacteria-inspired robotic microswimmers, Appl. Phys. Lett. **97**, 213704 (2010).

[6] W. Gao, D. Kagan, O. S. Pak, C. Clawson, S. Campuzano, E. Chuluun-Erdene, E. Shipton, E. E. Fullerton, L. Zhang, E. Lauga, and J. Wang, Cargo-towing fuel-free magnetic nanoswimmers for targeted drug delivery, Small **8**, 460 (2012).

[7] O. S. Pak, W. Gao, J. Wang, and E. Lauga, High-speed propulsion of flexible nanowire motors: Theory and experiments, Soft Matter **7**, 8169 (2011).

[8] I. S. M. Khalil, H. C. Dijkslag, L. Abelmann, and S. Misra, Magnetosperm: A microrobot that navigates using weak magnetic fields, Appl. Phys. Lett. **104**, 223701 (2014).

[9] B. Jang, E. Gutman, N. Stucki, B. F. Seitz, P. D. Wendel-García, T. Newton, J. Pokki, O. Ergeneman, S. Pané, Y. Or, and B. J. Nelson, Undulatory locomotion of magnetic multilink nanoswimmers, Nano Lett. **15**, 4829 (2015).

[10] E. Gutman and Y. Or, Simple model of a planar undulating magnetic microswimmer, Phys. Rev. E **90**, 013012 (2014).

[11] F. Alouges, A. De Simone, L. Giraldi, and M. Zoppello, Can magnetic multilayers propel artificial microswimmers mimicking sperm cells? Soft Robotics **2**, 117 (2015).

[12] B. J. Nelson, I. K. Kaliakatsos, and J. J. Abbott, Microrobots for minimally invasive medicine, Ann. Rev. Biomed. Eng. **12**, 55 (2010).

[13] G. Kósa and G. Székely, Swimming micro robots for medical applications, in *Surgical Robotics* (Springer, Berlin, 2011), pp. 369–395.

[14] S. Tottori, L. Zhang, F. Qiu, K. K. Krawczyk, A. Franco-Obregón, and B. J. Nelson, Magnetic helical micromachines: Fabrication, controlled swimming, and cargo transport, Adv. Mater. **24**, 811 (2012).

[15] O. Raz and A. M. Leshansky, Efficiency of cargo towing by a microswimmer, Phys. Rev. E **77**, 055305 (2008).

[16] R. Golestanian, Three-sphere low-Reynolds-number swimmer with a cargo container, Eur. Phys. J. E **25**, 1 (2008).

[17] B. U. Felderhof, Collinear swimmer propelling a cargo sphere at low Reynolds number, Phys. Rev. E **90**, 053013 (2014).

[18] A. Najafi and R. Golestanian, Simple swimmer at low Reynolds numbers: Three linked spheres, Phys. Rev. E **69**, 062901 (2004).

[19] E. Lauga, Floppy swimming: Viscous locomotion of actuated elastica, Phys. Rev. E **75**, 041916 (2007).

[20] E. E. Keaveny, S. W. Walker, and M. J. Shelley, Optimization of chiral structures for microscale propulsion, Nano Lett. **13**, 531 (2013).

[21] D. Walker, M. Kubler, K. I. Morozov, P. Fischer, and A. M. Leshansky, Optimal length of low Reynolds number nanopropellers, Nano Lett. **15**, 4412 (2015).

[22] M. Roper, R. Dreyfus, J. Baudry, M. Fermigier, J. Bibette, and H. A. Stone, Do magnetic micro-swimmers move like eukaryotic cells? Proc. Roy. Soc. London A **464**, 877 (2008).

[23] H. Gadêlha, On the optimal shape of magnetic swimmers, Regular and Chaotic Dyn. **18**, 75 (2013).

[24] E. M. Purcell, Life at low Reynolds number, Am. J. Phys. **45**, 3 (1977).

[25] See Supplemental Material at http://link.aps.org/supplemental/10.1103/PhysRevE.93.063105 for symbolic computation code.

[26] J. Gray and G. J. Hancock, The propulsion of sea-urchin spermatozoa, J. Exp. Biol. **32**, 802 (1955)

[27] R. G. Cox, The motion of long slender bodies in a viscous fluid part 1. general theory, J. Fluid Mech. **44**, 791 (1970).

[28] G. Fonnum, C. Johansson, A. Molteberg, S. Mørup, and E. Aksnes, Characterisation of dynabeads® by magnetization measurements and mössbauer spectroscopy, J. Magn. Magn. Mater. **293**, 41 (2005).